CARBON letters

Original Articles
Carbon Letters Vol. 16, No. 4, 233-240 (2015)

Electrochemical synthesis of nanosized hydroxyapatite/graphene composite powder

Vesna Mišković-Stanković[1,2], Sanja Eraković[1], Ana Janković[1], Maja Vukašinović-Sekulić[1], Miodrag Mitrić[3], Young Chan Jung[4], Soo Jin Park[5] and Kyong Yop Rhee[2,♠]

[1]Faculty of Technology and Metallurgy, University of Belgrade, Belgrade 11000, Serbia
[2]Department of Mechanical Engineering, Kyung Hee University, Yongin 17104, Korea
[3]Vinča Institute of Nuclear Sciences, University of Belgrade, Belgrade 11000, Serbia
[4]Korea Railroad Research Institute, Uiwang 16105, Korea
[5]Department of Chemistry, Inha University, Incheon 22212, Korea

Article Info
Received 21 July 2015
Accepted 15 September 2015

***Corresponding Author**
E-mail: rheeky@khu.ac.kr
Tel: +82-31-201-2565

Open Access
DOI: http://dx.doi.org/10.5714/CL.2015.16.4.233

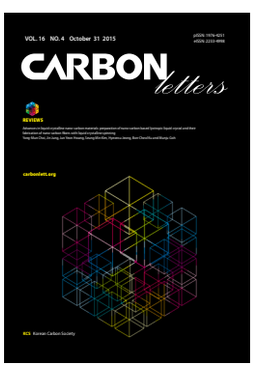

http://carbonlett.org

pISSN: 1976-4251
eISSN: 2233-4998

Abstract

Electrochemical synthesis was employed to prepare a novel hydroxyapatite/graphene (HAP/Gr) composite powder suitable for medical applications as a hard tissue implant (scaffold). The synthesis was performed in a homogeneous dispersion containing $Na_2H_2EDTA{\cdot}2H_2O$, NaH_2PO_4 and $CaCl_2$ with a Ca/EDTA/PO_4^{3-} concentration ratio of 0.25/0.25/0.15M, along with 0.01 wt% added graphene nanosheets, at a current density of 137 mA cm^{-2} and pH value of 9.0. The field emission scanning electron microscopy and transmission electron microscopy observations of the composite HAP/Gr powder indicated that nanosized hydroxyapatite particles were uniformly placed in the graphene overlay. Raman spectroscopy, Fourier transform infrared spectroscopy and X-ray diffraction confirmed graphene incorporation in the HAP/Gr powder. The electrochemically prepared HAP/Gr composite powder exhibited slight antibacterial effect against the growth of the bacterial strain *Staphylococcus aureus*.

Key words: graphene, hydroxyapatite, electrochemical synthesis, composites, antibacterial activity

1. Introduction

Graphene (Gr) is a one atom thick two-dimensional lattice where sp^2-hybridized carbon atoms are arranged in a flat honeycomb manner. It has drawn attention in the composite materials field as a useful reinforcement for composites due to its unique qualities: excellent thermal and mechanical properties, large specific surface area and electrical conductivity [1-3]. Graphene has been utilized as a new material in applications including field-effect transistors, memory devices, photovoltaic devices, electron acceptors, various sensors [3], and composites [4-7].

Even though graphene was originally developed for nanoelectronics applications [8], recent research has reported that graphene also has a significant potential in biomedical applications [9]. It has shown great prospects as a filler in bone tissue engineering, while interaction with biomaterials has rarely been reported [2]. In order to minimize direct metal-body fluid contact and to limit the undesired release of metallic ions into the body, biocompatible coatings on the metallic substrate, such as hydroxyapatite ($Ca_{10}(PO_4)_2(OH)_2$, HAP), have been suggested by many researchers [10-13]. As a major component of natural bone tissues, hydroxyapatite is chemically similar to the natural mineral in bone and has excellent biocompatibility; therefore it is very suitable as an orthopedic biomaterial in various forms and shapes for bone growth and integration [1].

To overcome the poor mechanical properties of hydroxyapatite, our previous research

focused on applying graphene in HAP/Gr composite coatings on titanium substrates [14,15]. Recent studies employing graphene as an ideal reinforcement material for hydroxyapatite have demonstrated the significant toughness and strength of the composites, which retain their biocompatibility without any offsetting bioactivity [1,14-16]. It is worth mentioning that, for biomedical purposes, graphene has been used along with chitosan in composites that reportedly show a 200 times increase in elasticity modulus compared to undoped chitosan [17]. Also, it has been reported that the superior electrical conductivity of graphene stimulates the adhesion and proliferation of osteoblasts during new tissue growth [2]. Crack deflection is more effective when using sheet-like reinforcement, as compared with tubular-like reinforcement, suggesting that graphene nano-sheets (GNSs) exhibit a more pronounced toughening effect on brittle materials than do carbon nanotubes (CNTs) [18]. Unlike CNTs, Gr has been synthesized in relatively pure ways and is expected to exhibit low cytotoxicity, since few metallic catalyst particles are associated with its production [19,20]. Therefore, the investigation of graphene-based nanomaterials, and their biomedical application in particular, is an exciting new field of research [21].

The presence of implant materials inside the human body can interfere with the host immune response, and microorganisms have opportunity to adhere to the implant surface, forming so-called biofilms [22]. The antimicrobial properties of graphene-based materials have been thoroughly evaluated by many researchers [22-25]. The antibacterial activity of graphene oxide and graphene is attributed to the significant membrane stress induced by the sharp edges of their nanosheets, which may result in physical damage to cell membranes, leading to the loss of bacterial membrane integrity and the leakage of RNA [25,26]. GNSs serve as "cutters" to disrupt and damage bacteria cell membranes, consisting of phospholipid molecules, leading to the release of bacterial intracellular contents into the environment and eventually bacterial death [25].

The aim of this work was to electrochemically synthesize HAP/Gr composite powder under constant current density for medical aplications as a hard tissue implant (scaffold), and to investigate its antibacterial effect against the growth of bacterial strains, including *Staphylococcus aureus*. Here, we utilized the specific chemical characteristics of ethylenediaminetetraacetic acid (EDTA, $C_{10}H_{16}N_2O_8$), since organic modifiers are widely used for the morphology and size controlled synthesis of hydroxyapatite [27]. The solubility of graphene in aqueous environment was surpassed functionalizing GNSs by EDTA under specific synthesis conditions [28].

2. Experimental

2.1. Materials and sample preparation

A homogeneous aqueous dispersion with a final volume of 200 mL, containing $Na_2H_2EDTA{\cdot}2H_2O$, NaH_2PO_4 and $CaCl_2$ ($Ca/EDTA/PO_4^{3-}$ = 0.25/0.25/0.15 M) and 0.01 wt% graphene was used. The $Na_2H_2EDTA{\cdot}2H_2O$, NaH_2PO_4 and $CaCl_2$ chemicals were all reagent grade (Sigma Aldrich Chemie, Munich, Germany) and used without further purification. The graphene nanopowder (AO-3) was purchased from Graphene Supermarket, USA. The average thickness of the graphene nanoflakes was 12 nm. Approximately 30-50 layers of graphene monolayers were overlapped together. The pH value of the as-received dispersion was 2.0, subsequently titrated with 10 M NaOH to pH 9.0 with an appropriate amount of NaOH.

Subsequently, HAP/Gr powder was synthesized galvanostatically in a two-electrode cell (two rectangular Pt electrodes, 10 mm × 10 mm) at an applied current density of 137 mA cm^{-2}, with constant stirring at room temperature for 3 h, using Reference 600 Potentiostat/Galvanostat/ZRA (Gamry Instruments Inc., Warminster, PA, USA). After that the dispersion was kept at 40°C until a dense precipitate was obtained. The precipitate was rinsed with deionized water and spun down several times in a centrifuge (10,000 rpm) until a negative reaction for Cl^- ions with $AgNO_3$ was observed. The final HAP/Gr powder was obtained by drying for 48 h at room temperature.

2.2. Characterization

The morphology of the HAP/Gr powder was analyzed by field emission scanning electron microscopy (FE-SEM), conducted on a LEO SUPRA 55 (Carl Zeiss, Oberkochen, Germany) operated at an acceleration voltage of 200 kV. Transmission electron microscopy (TEM) measurements of the HAP/Gr powder were carried out using a JEOL 100CX microscope instrument at an operating voltage of 100 kV. Samples were prepared by placing a drop of diluted aqueous HAP/Gr suspension onto a carbon-coated copper grid, and dried samples were examined by TEM. HR-Raman analysis was used to verify graphene incorporation into the composite HAP/Gr powder. This analysis was carried out using a inVia Raman spectrophotometer (Renishaw) equipped with a 514 nm argon laser with 10% intensity of total power (50 mW) and the spectral range of 100 to 3500 cm^{-1}. X-ray diffraction analysis (XRD) was used to assess the phase composition of the HAP/Gr powder. XRD intensity was measured by Philips PW 1051 powder diffractometer, with Ni filtered CuK_α radiation (λ = 1.5418 Å), using a scan-step technique (2θ = 8°-80°), with a scanning step width of 0.05° and exposure time of 50 s per step. The phase analysis was done by computer program EVA V.9.0 (PDF-2 database). Thermogravimetric analysis (TGA) to assess the thermal stability of the HAP/Gr powder was carried out by TGA Q5000 IR/SDT Q600, from 25°C to 600°C under nitrogen atmosphere (50 mL/min) at a heating rate of 20 °C/min. Infrared spectra were collected by a Nicolet iS50 FT-IR spectrometer (Thermo Scientific, Waltham, MA, USA), using the KBr technique, in the range 4000-400 cm^{-1} and 4 cm^{-1} resolution averaging 32 scans.

2.3. Antibacterial activity

The antibacterial activity of the HAP/Gr composite powder was tested against the Gram-positive pathogenic bacteria strain *S. aureus* TL (culture collection-FTM, University of Belgrade, Belgrade, Serbia) and Gram-negative bacteria strain *Escherichia coli* (ATCC 25922) in suspension using the spread-plate method. The inoculums of all microorganisms were prepared from fresh overnight LB broth (10 g/L tryptone, 5 g/L yeast extract, 5 g/L NaCl) cultures incubated at 37°C.

Overnight cultures (*S. aureus* and *E. coli*) were diluted in a

physiological solution (10^{-1}). The starting bacterial culture, 10^4-10^5 CFU mL^{-1}, was exposed to the synthesized powder, at a concentration of 2 mg mL^{-1}, in a phosphate-buffered (PB) solution (pH = 7.4). Then the prepared samples were incubated for 24 h at 37°C with shaking, and aliquots were taken at 0, 1, 3 and 24 h. The samples were serially diluted, and 100 μL of the appropriate dilutions were mixed with 20 mL of melted LB agar (temperature 55°C) and poured into a petri dish. After 24 h incubation at 37°C, plates containing 25 to 250 colonies were enumerated using a colony counter and expressed as CFU mL^{-1} to obtain the number of viable *S. aureus* and *E. coli* in each sample.

3. Results and Discussion

3.1. Morphological characterization

The surface morphology, size and quality of the prepared composite HAP/Gr powder was investigated by TEM and FE-SEM analysis. It can be clearly seen from the TEM results (Fig. 1) that the Gr surface is highly modified, which confirms the EDTA functionalization on its surface. The FE-SEM image (Fig. 2, under high magnification of ×100,000) displays the formation of thick nano-sheets with wrinkled morphology, which is in good agreement with the TEM image.

The results are a solid indication that Gr acts effectively as a nano-reinforcement filler, by providing frictional pull out, crack deflection, and crack bridging as the major toughening mechanisms to resist crack propagation [1]. The high specific surface area of the graphene nanosheets creates an increased contact area with the hydroxyapatite matrix, significantly enhancing the bonding strength between the graphene and hydroxyapatite grains. Moreover, the rough and wrinkled surface texture of the graphene nanosheets plays an important role in enhancing mechanical interlocking, leading to increased load-transfer efficiency between the hydroxyapatite matrix and graphene nanosheets. Finally, it was shown that the two ends of the graphene nanosheets are well bonded to the adjacent hydroxyapatite grains with the plane of the graphene nanosheets nearly parallel to the fracture surface. Thus, it is hypothesized that the grain bridging by graphene nanosheets has a fundamental role in inhibiting crack propagation along the grain boundary (grain-boundary toughening mechanism).

Fig. 1. Transmission electron microscopy microphotograph of hydroxyapatite/graphene (HAP/Gr) composite powder.

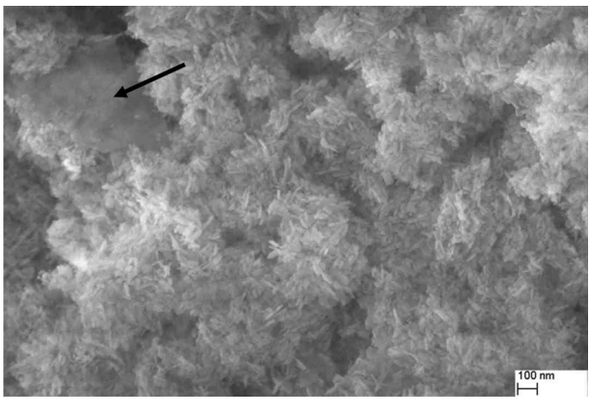

Fig. 2. Field emission scanning electron microscopy microphotograph of hydroxyapatite/graphene (HAP/Gr) composite powder (the black arrow points out Gr embedded on and surrounded by the hydroxyapatite grains).

The FE-SEM microphotographs also revealed the surface homogenicity of the electrochemically prepared HAP/Gr powder, which consisted of big agglomerates composed of fine plate-like crystallites of ~40 nm. A similar morphology was observed in the case of electrochemically pure hydroxyapatite powder obtained at the same current density and pH value [29]. The agglomerates of hydroxyapatite nanoparticles, evident in the TEM images shown in Fig. 1, are embedded in a transparent overlay of graphene sheets.

Additionaly, the FE-SEM image (Fig. 2) of prepared composite powder showed that the graphene was surrounded by clusters of plate-like hydroxyapatite nanoparticles (marked with an arow in the high magnification image). In our previous work we have established that hydroxyapatite nanoparticles have a strong tendency to agglomerate due to their high surface area and energy [29].

3.2. XRD, Raman and FT-IR analysis

The XRD pattern of the HAP/Gr composite powder (Fig. 3) demonstrates that the predominately detected crystalline phase is assigned to hydroxyapatite. High intensity hydroxyapatite peaks at crystal planes (002), (211), (112), and (300) at 2θ = 26.0°, 31.9°, 32.1°, and 32.9°, respectively, match perfectly to the Joint Committee on Powder Diffraction Standards (JCPDS) standard PDF card No. 01-86-1199 for hydroxyapatite.

According to Ju et al. [30], thermally-reduced graphenes showed a broad (002) peak at 2θ = 23°~26° [30,31]. However, in our case, the Gr diffraction peaks are mostly shielded by hydroxyapatite peaks, since the strong diffraction peak for the hydroxyapatite crystal plane (002) is evident at 2θ = 26.0°. In addition, the specific weak broad peak at 2θ~23° observed for pure Gr (starting compound AO-3, data not shown) is also overlapped by diffraction peaks originating from the hydroxyapatite. Finally, the carbon peak at 2θ = 26.6° is assigned to the carbon crystal (002) plane, as it appears in Fig. 3, and is attributed to the starting carbon material, as per the manufacturer specification (AO-3, Graphene Supermarket).

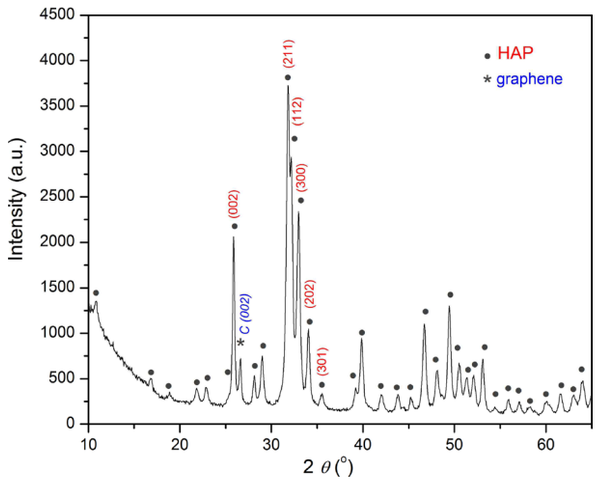

Fig. 3. X-ray diffraction analysis pattern of hydroxyapatite/graphene (HAP/Gr) composite powder.

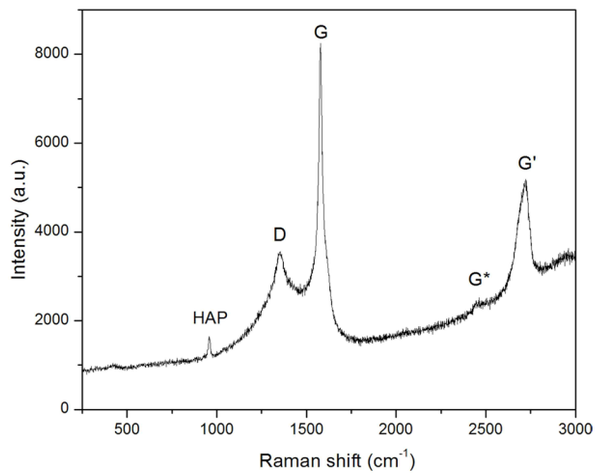

Fig. 4. Raman spectrum of hydroxyapatite/graphene (HAP/Gr) composite powder.

Using the X-ray line profile fitting program with a fundamental parameters convolution approach for generating line profiles [32], we calculated the coherent domain sizes and microstrain of HAP/Gr using the (002), (211), (112), (300), (202), and (301) crystal planes. The crystallite domain size, calculated to be 28.9 nm, indicates that the agglomerates observed by FE-SEM analysis were formed through the drying process. This is in good agreement with the proposed nucleation-aggregation-agglomeration growth mechanism [33]. According to this mechanism, particle formation occurs in the following steps: (1) nucleation and growth to form crystallites in nanometric size range, (2) aggregation of elemental nanocrystals by physical attractions, and (3) further crystal growth to form stable agglomerates. However, the presence of Gr increased the crystalline domain size of the hydroxyapatite grains, since the reported value for pure hydroxyapatite electrochemically synthesized at the same pH and current density was 21.6 nm [29], indicating that there were interactions between the hydroxyapatite and graphene sheets.

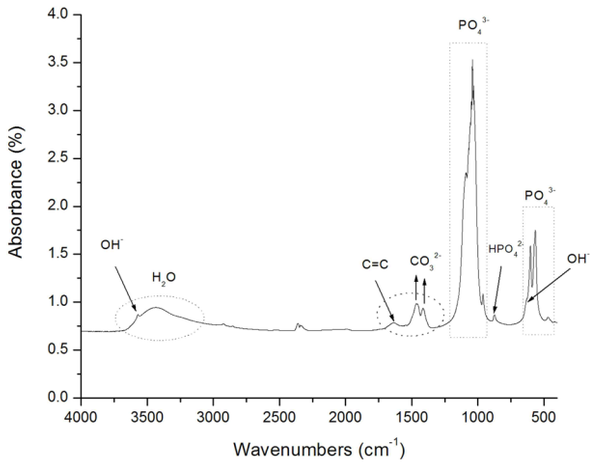

Fig. 5. Fourier transform infrared spectroscopy spectrum of hydroxyapatite/graphene (HAP/Gr) composite powder.

Raman measurement was employed to identify the existence of Gr in the composite powder. The Raman spectrum of the HAP/Gr powder (Fig. 4) depicts both the typical D peak at 1350 cm^{-1} and the G peak at 1578 cm^{-1}, as well as the very weak G* peak at 2434 cm^{-1} and G' peak at 2715 cm^{-1}, denoted as a major fingerprint of graphene structure [34]. The shape, position and intensity of the G' band depends markedly on the number of layers. The G-band corresponds to the ordered sp^2-bonded carbon atoms and the D-band represents defects originating from the disordered aromatic structure on the Gr edges [35]. The characteristic sharp Raman peak at 961 cm^{-1} is characteristic of the nanosized crystalline hydroxyapatite phase, which is attributed to the symmetric stretching mode $\nu_1(PO_4^{3-})$ [36]. The Raman study therefore indicates the interaction between Gr and hydroxyapatite, confirming the integration of graphene in the novel electrochemically prepared HAP/Gr composite powder.

The Fourier transform infrared spectroscopy (FT-IR) spectrum of the HAP/Gr powder is depicted in Fig. 5 indicating the characteristic absorption bands of natural hydroxyapatite at 463, 569 and 603 cm^{-1}, which are attributed to the P−O bending of phosphate groups [37]. The three absorption bands of the PO_4^{3-} group were clearly distinguished in the composite HAP/Gr nanopowder at 1092, 1038 and 960 cm^{-1}, which corresponds to the O−P−O phosphate ions of the hydroxyl site [38,39]. The characteristic band at 3572 cm^{-1} and weak broad band at 634 cm^{-1} can be attributed to the stretching and vibrational modes of the structural OH^- groups of the hydroxyapatite lattice [40]. The absorbance bands at 1420 and 1460 cm^{-1} correspond to ν_3 asymmetrical stretching vibrations of the CO_3^{2-} ions, indicating predominatly B-type hydroxyapatite [41]. It is preferential substitution in the human bone known for its excellent bioactivity and osteoinductivity [41]. A vibration band located at 1640 cm^{-1} corresponds to the skeletal vibration of Gr due to aromatic sp^2 hybridized C=C vibration stretching [38,39,42], confirming its presence in the synthesized composite.

The mechanism of hydroxyapatite formation requires the liberation of Ca^{2+} ions from EDTA [29,43]:

$$Ca(EDTA)^{2-} \leftrightarrows Ca^{2+} + EDTA^{4-} \quad (1)$$

the generation of OH^- ions through water reduction:

$$2H_2O + 2e^- \rightarrow H_2 + 2OH^- \quad (2)$$

and ionic migration towards the electrodes, where precipitation of hydroxyapatite occurs:

$$10Ca^{2+} + 6PO_4^{3-} + 2OH^- \leftrightarrows Ca_{10}(PO_4)_6(OH)_2 \quad (3)$$

As previously emphasized, the role of EDTA is to provide a functionalized surface on the Gr sheets, where the nucleation of hydroxyapatite grains is facilitated. However, hydroxyapatite nanorods grow with a preferred orientation along the graphene sheets. According to Liu et al. [21], the hydroxyapatite and graphene sheets are connected by van der Waals bonding. Nucleation of the hydroxyapatite crystals probably occurs on either the graphene wall or the cross-section of graphene multi-sheets, followed by subsequent crystal growth along or perpendicular to the surface of the graphene sheet. They proved that the (300) plane of the hydroxyapatite crystals is parallel to the surface of the graphene walls.

Keeping in mind the atomic structure of hydroxyapatite, the (300) plane contains Ca atoms at each corner of the rectangle and the distance between each pair of Ca atoms is 0.9418 nm and 0.6884 nm, whereas the distance between two neighboring Ca atoms in the (100) plane is 0.9418 nm and 0.3442 nm, respectively, while the distance between adjacent graphene sheets is 0.347 nm. Single layer graphene is constituted by carbon atoms arranged periodically in a hexagonal manner, and the nearest distance between two carbon atoms is 0.142 nm. Multilayer graphene sheets contain several graphene monolayers with the inter-wall distance of 0.340 nm. On the other hand**,** the lattice spacing of the (002) plane of hydroxyapatite is 0.344 nm. Since the (300) plane takes priority over the (100) plane to match with the surface of the graphene sheets, and the open ends of the graphene multisheets form relatively stronger interfaces with the (002) plane of the hydroxyapatite crystals than other planes, it can be considered that the (300) plane of the hydroxyapatite forms a strong interfacial bond with the surface of the graphene wall, and the cross-section of graphene builds a strong interface with the (002) plane of the HAP crystals due to the smaller lattice mismatch.

Therefore, all of the above analyses—XRD, FT-IR and Raman spectroscopy—confirm the incorporation of graphene in the prepared HAP/Gr powder.

3.3. Thermal properties

TGA was conducted in order to study the decomposition behavior and phase transformation of the HAP/Gr composite. Fig. 6 depicts the differential thermogravimetry (DTG) and TG curves of nanosized HAP/Gr powder in the temperature range 25°C-600°C, exhibiting three weight loss stages. The first stage from 25°C to 170°C, with 2.32 wt% mass loss and a sharp peak in the DTG curve at 73°C, corresponds to the desorption of adsorbed water molecules from the crystallite surface. The second stage (170°C-420°C), with 2.60 wt% mass loss and a broad peak at around 300°C in the DTG curve, corresponds to the combustion of the organic material, EDTA [44] and the unstable carbon in the graphene structure [45], as well as the beginning of hydroxyapatite dehydroxylation [14,15]. The third stage, observed between 420°C and 600°C, with 1.22 wt. % mass loss and a peak at 485°C in the DTG curve, is attributed to the complete decomposition of graphene [46] and the dehydroxylation or early slow decomposition of hydroxyapatite [29]. The total mass loss at 600ºC was 6.14 wt%, confirming the greater thermal stability of the nanosized HAP/Gr powder, compared to 9.50 wt% mass loss for pure hydroxyapatite synthesized under the same conditions.

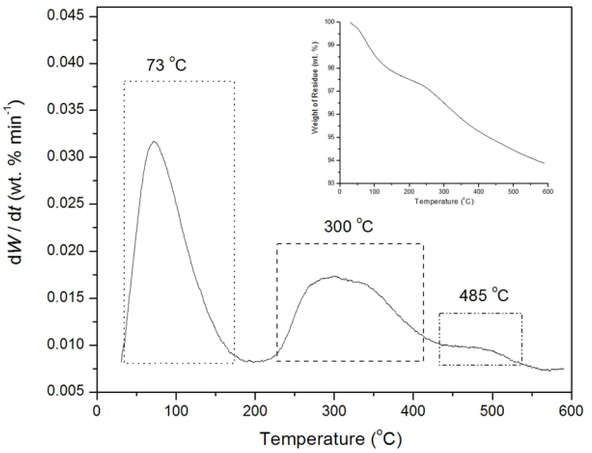

Fig. 6. Differential thermogravimetry (TG) and TG (inset) curves of hydroxyapatite/graphene (HAP/Gr) composite powder.

3.4. Antibacterial efficacy

The antibacterial activity of the HAP/Gr powder was investigated quantitatively against two bacterial strains, Gram-positive *S. aureus* and Gram-negative *E. coli*, by monitoring the changes in the viable number of bacterial cells in suspension in the presence of hydroxyapatite (as a reference) and HAP/Gr powder,s in comparison to a control without any material. Fig. 7 depicts the number of viable cells of *S. aureus* and *E.coli* in PB solution.

A slight decrease in the total number of *S. aureus* cells 1 h post-incubation was noticed for the HAP/Gr powders (Fig. 7a) when compared to the initial number of cells in suspensions. On the other hand, according to the antibacterial assays, the antibacterial efficacy of the HAP/Gr powder could not be confirmed to prevent *E. coli* growth (Fig. 7b).

The antibacterial mechanism of the HAP/Gr powder can be understood as a result of the graphene-based materials causing direct damage to cell membranes and/or by oxidative stress. Namely, bacterial viability decreases as a result of graphene causing direct physical damage to bacterial membranes and finally resulting in the release of intracellular contents. This breach in the cell wall is caused by the blade-like action of low thickness graphene with sharp edges [25,47]. In addition, graphenes may chemically increase cellular oxidative stress, which could disrupt a specific microbial process. Oxidative stress mediated by the graphene-based materials could have several

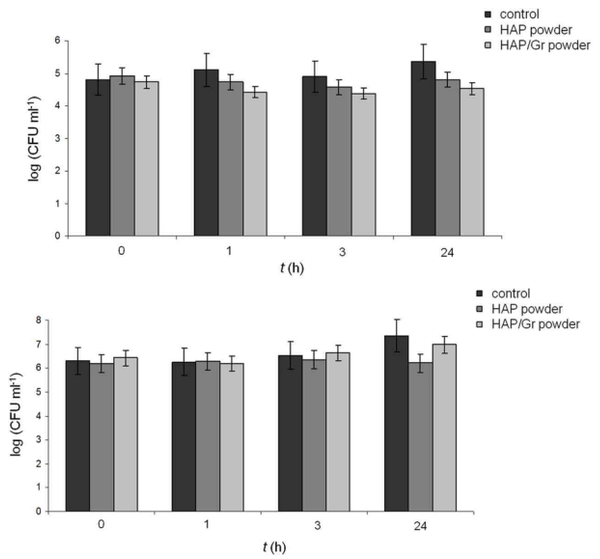

Fig. 7. Reduction of viable cell number of *Staphylococcus aureus* (a) and *Escherichia coli* (b) after contact with HAP and hydroxyapatite/graphene (HAP/Gr) powders for 0, 1, 3 and 24 h in phosphate-buffered as compared to the control w/o samples.

different routes. The first one is through formation of reactive oxygen species (ROS), whereby oxidative stress is induced by ROS generated by graphene and related species, e.g. graphene oxide or reduced graphene oxide. The other possibility is ROS-independent oxidative stress. Graphene-based materials may target a specific microbial process or a vital cellular structure or component by disturbing them or oxidizing, without ROS production [25].

Both of these effects are enhanced in the reduced form of the materials (pure graphene), due to the stronger interaction between sharp sheet edges and the bacteria's cell membrane and/or better charge transfer between the bacteria and the graphene-based material itself.

Based on our antimicrobial results, the investigated HAP/Gr composite powder could be considered a selective antibacterial material. Selectivity and specificity, targeting specific bacterial strains, are mandatory requirements for any type of antibiotic medication. Even though its present efficacy needs improving, the HAP/Gr composite powder is a candidate for a selective biomaterial for bone tissue engineering. However, since the antibacterial activity of graphene remains a controversial issue [47], further insights into the mechanism of graphene antibacterial action are needed and should be further pursued. To ensure the strong antibacterial activity of the HAP/Gr composite, the addition of small quantities of silver nanoparticles is necessary, as we proved in our previous work [15].

4. Conclusions

In summary, we demonstrated the succesful electrochemical synthesis of nanosized composite HAP/Gr powder at constant current density. Agglomerates of HAP/Gr nanoparticles in the graphene overlayer were observed by FE-SEM and TEM analysis. Raman spectra provided evidence of the characteristic D, G, G* and fingerprint G' (2715 cm^{-1}) bands, indicating that the graphene retained its original structure in the HAP/Gr powder. XRD analysis proved Gr incorporation, and the increase in the crystalline domain size of HAP/Gr in comparison to pure hydroxyapatite powder, due to established interactions between the hydroxyapatite and graphene sheets, which was also confirmed by the composite's greater thermal stability. The FT-IR spectrum revealed the vibration band located at 1640 cm^{-1} which corresponds to aromatic sp^2 hybridized C=C vibration stretching, as expected for HAP/Gr. The absorbance bands indicated predominatly carbonate B-type hydroxyapatite, identical to the human bone and therefore an ideal substitution material with excellent bioactivity and osteoinductivity. The electrochemically synthesized HAP/Gr powder exhibited a slight antibacterial effect against *S. aureus* growth and no activity against *E. coli* growth. These results could pave the way for producing the electrochemically fabricated nanosized HAP/Gr powder with an antimicrobial dopand for improved antibacterial activity, as a potential biomaterial for bone tissue engineering.

Acknowledgments

This work was supported by the Basic Science Research Program through the National Research Foundation of Korea (NRF) funded by the Ministry of Education, Science and Technology (project number: 2013R1A1A2A10063466). This research was also financed by the Ministry of Education, Science and Technological Development, Republic of Serbia, contract No. III 45019.

The authors would like to thank Dr. Nataša Bibić, Vinča Institute of Nuclear Sciences, University of Belgrade, for performing TEM analysis.

References

[1] Zhang L, Liu W, Yue C, Zhang T, Li P, Xing Z, Chen Y. A tough graphene nanosheet/hydroxyapatite composite with improved in vitro biocompatibility. Carbon, **61,** 105 (2013). http://dx.doi.org/10.1016/j.carbon.2013.04.074.

[2] Kim S, Ku SH, Lim SY, Kim JH, Park CB. Graphene-biomineral hybrid materials. Adv Mater, **23,** 2009 (2011). http://dx.doi.org/10.1002/adma.201100010.

[3] Chavez-Valdez A, Shaffer MSP, Boccaccini AR. Applications of graphene electrophoretic deposition. J Phys Chem B, **117,** 1502 (2013). http://dx.doi.org/10.1021/jp3064917.

[4] Wang Z, Wei P, Qian Y, Liu J. The synthesis of a novel graphene-based inorganic–organic hybrid flame retardant and its application in epoxy resin. Compos Part B Eng, **60,** 341 (2014). http://dx.doi.org/10.1016/j.compositesb.2013.12.033.

[5] Uddin ME, Layek RK, Kim NH, Hui D, Lee JH. Preparation and properties of reduced graphene oxide/polyacrylonitrile nanocomposites using polyvinyl phenol. Compos Part B Eng, **80,** 238 (2015). http://dx.doi.org/10.1016/j.compositesb.2015.06.009.

[6] Kim M, Kim Y, Baeck SH, Shim SE. Effect of surface treatment of graphene nanoplatelets for improvement of thermal and electrical properties of epoxy composites. Carbon Lett, **16,** 34 (2015). http://

dx.doi.org/10.5714/CL.2015.16.1.034.

[7] Bose S, Drzal LT. Functionalization of graphene nanoplatelets using sugar azide for graphene/epoxy nanocomposites. Carbon Lett, **16,** 101 (2015). http://dx.doi.org/ 10.5714/CL.2015.16.2.101.

[8] Kopelevich Y, Esquinazi P. Graphene physics in graphite. Adv Mater, **19,** 4559 (2007). http://dx.doi.org/10.1002/adma.200702051.

[9] Fabbri P, Valentini L, Hum J, Detsch R, Boccaccini AR. 45S5 Bioglass®-derived scaffolds coated with organic-inorganic hybrids containing graphene. Mater Sci Eng C, **33,** 3592 (2013). http://dx.doi.org/10.1016/j.msec.2013.04.028.

[10] Kung KC, Lee TM, Lui TS. Bioactivity and corrosion properties of novel coatings containing strontium by micro-arc oxidation. J Alloys Compd, **508,** 384 (2010). http://dx.doi.org/10.1016/j.jallcom.2010.08.057.

[11] Rath PC, Besra L, Singh BP, Bhattacharjee S. Titania/hydroxyapatite bi-layer coating on Ti metal by electrophoretic deposition: characterization and corrosion studies. Ceram Int, **38,** 3209 (2012). http://dx.doi.org/10.1016/j.ceramint.2011.12.026.

[12] Geetha M, Singh AK, Asokamani R, Gogia AK. Ti based biomaterials, the ultimate choice for orthopaedic implants: a review. Prog Mater Sci, **54,** 397 (2009). http://dx.doi.org/10.1016/j.pmatsci.2008.06.004.

[13] Swetha M, Sahithi K, Moorthi A, Srinivasan N, Ramasamy K, Selvamurugan N. Biocomposites containing natural polymers and hydroxyapatite for bone tissue engineering. Int J Biol Macromol, **47,** 1 (2010). http://dx.doi.org/10.1016/j.ijbiomac.2010.03.015.

[14] Janković A, Eraković S, Mitrić M, Matić IZ, Juranić ZD, Tsui GCP, Tang C, Mišković-Stanković V, Rhee KY, Park SJ. Bioactive hydroxyapatite/graphene composite coating and its corrosion stability in simulated body fluid. J Alloys Compd, **624,** 148 (2015). http://dx.doi.org/10.1016/j.jallcom.2014.11.078.

[15] Janković A, Eraković S, Vukašinović-Sekulić M, Mišković-Stanković V, Park SJ, Rhee KY. Graphene-based antibacterial composite coatings electrodeposited on titanium for biomedical applications. Prog Org Coat, **83,** 1 (2015). http://dx.doi.org/10.1016/j.porgcoat.2015.01.019.

[16] Liu H, Xi P, Xie G, Shi Y, Hou F, Huang L, Chen F, Zeng Z, Shao C, Wang J. Simultaneous reduction and surface functionalization of graphene oxide for hydroxyapatite mineralization. J Phys Chem C, **116,** 3334 (2012). http://dx.doi.org/10.1021/jp2102226.

[17] Fan H, Wang L, Zhao K, Li N, Shi Z, Ge Z, Jin Z. Fabrication, mechanical properties, and biocompatibility of graphene-reinforced chitosan composites. Biomacromolecules, **11,** 2345 (2010). http://dx.doi.org/10.1021/bm100470q.

[18] Rafiee MA, Rafiee J, Srivastava I, Wang Z, Song H, Yu ZZ, Koratkar N. Fracture and fatigue in graphene nanocomposites. Small, **6,** 179 (2010). http://dx.doi.org/10.1002/smll.200901480.

[19] Lahiri D, Ghosh S, Agarwal A. Carbon nanotube reinforced hydroxyapatite composite for orthopedic application: a review. Mater Sci Eng C, **32,** 1727 (2012). http://dx.doi.org/10.1016/j.msec.2012.05.010.

[20] Park S, Ruoff RS. Chemical methods for the production of graphenes. Nat Nanotechnol, **4,** 217 (2009). http://dx.doi.org/10.1038/nnano.2009.58.

[21] Liu Y, Huang J, Li H. Synthesis of hydroxyapatite-reduced graphite oxide nanocomposites for biomedical applications: oriented nucleation and epitaxial growth of hydroxyapatite. J Mater Chem B, **1,** 1826 (2013). http://dx.doi.org/10.1039/C3TB00531C.

[22] de Faria AF, Martinez DST, Meira SMM, de Moraes ACM, Brandelli A, Filho AGS, Alves OL. Anti-adhesion and antibacterial activity of silver nanoparticles supported on graphene oxide sheets. Colloids Surf B Biointerfaces, **113,** 115 (2014). http://dx.doi.org/10.1016/j.colsurfb.2013.08.006.

[23] Akhavan O, Ghaderi E, Esfandiar A. Wrapping bacteria by graphene nanosheets for isolation from environment, reactivation by sonication, and inactivation by near-infrared irradiation. J Phys Chem B, **115,** 6279 (2011). http://dx.doi.org/10.1021/jp200686k.

[24] Santos CM, Mangadlao J, Ahmed F, Leon A, Advincula RC, Rodrigues DF. Graphene nanocomposite for biomedical applications: fabrication, antimicrobial and cytotoxic investigations. Nanotechnology, **23,** 395101 (2012). http://dx.doi.org/10.1088/0957-4484/23/39/395101.

[25] Liu S, Zeng TH, Hofmann M, Burcombe E, Wei J, Jiang R, Kong J, Chen Y. Antibacterial activity of graphite, graphite oxide, graphene oxide, and reduced graphene oxide: membrane and oxidative stress. ACS Nano, **5,** 6971 (2011). http://dx.doi.org/10.1021/nn202451x.

[26] Das S, Singh S, Singh V, Joung D, Dowding JM, Reid D, Anderson J, Zhai L, Khondaker SI, Self WT, Seal S. Oxygenated functional group density on graphene oxide: its effect on cell toxicity. Part Part Syst Charact, **30,** 148 (2013). http://dx.doi.org/10.1002/ppsc.201200066.

[27] Kanchana P, Sekar C. EDTA assisted synthesis of hydroxyapatite nanoparticles for electrochemical sensing of uric acid. Mater Sci Eng C, **42,** 601 (2014). http://dx.doi.org/10.1016/j.msec.2014.05.072.

[28] Shruthi TK, Ilayaraja N, Jeyakumar D, Sathish M. Functionalization of graphene with nitrogen using ethylenediaminetetraacetic acid and their electrochemical energy storage properties. RSC Adv, **4,** 24248 (2014). http://dx.doi.org/10.1039/C4RA02756F.

[29] Djošić MS, Mišković-Stanković VB, Milonjić S, Kačarević-Popović ZM, Bibić N, Stojanović J. Electrochemical synthesis and characterization of hydroxyapatite powders. Mater Chem Phys, **111,** 137 (2008). http://dx.doi.org/10.1016/j.matchemphys.2008.03.045.

[30] Ju HM, Choi SH, Huh SH. X-ray diffraction patterns of thermally-reduced graphenes. J Korean Phys Soc, **57,** 1649 (2010). http://dx.doi.org/10.3938/jkps.57.1649.

[31] Sharma G, Gosavi SW. Thermoluminescence properties of graphene–nano ZnS composite. J Lumin, **145,** 557 (2014). http://dx.doi.org/10.1016/j.jlumin.2013.08.021.

[32] Cheary RW, Coelho A. A fundamental parameters approach to X-ray line-profile fitting. J Appl Crystallogr, **25,** 109 (1992). http://dx.doi.org/10.1107/S0021889891010804.

[33] Mostafa NY. Characterization, thermal stability and sintering of hydroxyapatite powders prepared by different routes. Mater Chem Phys, **94,** 333 (2005). http://dx.doi.org/10.1016/j.matchemphys.2005.05.011.

[34] Ouyang Y, Chen L. Surface-enhanced Raman scattering studies of few-layer graphene on silver substrate with 514 nm excitation. J Mol Struct, **992,** 48 (2011). http://dx.doi.org/10.1016/j.molstruc.2011.02.030.

[35] Nguyen VH, Kim BK, Jo YL, Shim JJ. Preparation and antibacterial activity of silver nanoparticles-decorated graphene composites. J Supercrit Fluids, **72,** 28 (2012). http://dx.doi.org/10.1016/j.supflu.2012.08.005.

[36] Zanin H, Saito E, Marciano FR, Ceragioli HJ, Granato AEC, Porcionatto M, Lobo AO. Fast preparation of nano-hydroxyapatite/

superhydrophilic reduced graphene oxide composites for bioactive applications. J Mater Chem B Biol Med, **1,** 4947 (2013). http://dx.doi.org/10.1039/C3TB20550A.

[37] Oyefusi A, Olanipekun O, Neelgund GM, Peterson D, Stone JM, Williams E, Carson L, Regisford G, Oki A. Hydroxyapatite grafted carbon nanotubes and graphene nanosheets: promising bone implant materials. Spectrochim Acta A Mol Biomol Spectrosc, **132,** 410 (2014). http://dx.doi.org/10.1016/j.saa.2014.04.004.

[38] Baradaran S, Moghaddam E, Basirun WJ, Mehrali M, Sookhakian M, Hamdi M, Nakhaei Moghaddam MR, Alias Y. Mechanical properties and biomedical applications of a nanotube hydroxyapatite-reduced graphene oxide composite. Carbon, **69,** 32 (2014). http://dx.doi.org/10.1016/j.carbon.2013.11.054.

[39] Neelgund GM, Oki A, Luo Z. In situ deposition of hydroxyapatite on graphene nanosheets. Mater Res Bull, **48,** 175 (2013). http://dx.doi.org/10.1016/j.materresbull.2012.08.077.

[40] Li M, Liu Q, Jia Z, Xu X, Shi Y, Cheng Y, Zheng Y, Xi T, Wei S. Electrophoretic deposition and electrochemical behavior of novel graphene oxide-hyaluronic acid-hydroxyapatite nanocomposite coatings. Appl Surf Sci, **284,** 804 (2013). http://dx.doi.org/10.1016/j.apsusc.2013.08.012.

[41] Wu CC, Huang ST, Tseng TW, Rao QL, Lin HC. FT-IR and XRD investigations on sintered fluoridated hydroxyapatite composites. J Mol Struct, **979,** 72 (2010). http://dx.doi.org/10.1016/j.molstruc.2010.06.003.

[42] Ren Y, Fan G, Wang C. Aqueous hydrodechlorination of 4-chlorophenol over an Rh/reduced graphene oxide synthesized by a facile one-pot solvothermal process under mild conditions. J Hazard Mater, **274,** 32 (2014). http://dx.doi.org/10.1016/j.jhazmat.2014.04.005.

[43] Fujishiro Y, Fujimoto A, Sato T, Okuwaki A. Coating of hydroxyapatite on titanium plates using thermal dissociation of calcium-EDTA chelate complex in phosphate solutions under hydrothermal conditions. J Colloid Interface Sci, **173,** 119 (1995). http://dx.doi.org/10.1006/jcis.1995.1304.

[44] Bogdanoviciene I, Beganskiene A, Tõnsuaadu K, Glaser J, Meyer HJ, Kareiva A. Calcium hydroxyapatite, Ca10(PO4)6(OH)2 ceramics prepared by aqueous sol–gel processing. Mater Res Bull, **41,** 1754 (2006). http://dx.doi.org/10.1016/j.materresbull.2006.02.016.

[45] Loryuenyong V, Totepvimarn K, Eimburanapravat P, Boonchompoo W, Buasri A. Preparation and characterization of reduced graphene oxide sheets via water-based exfoliation and reduction methods. Adv Mater Sci Eng, **2013,** 923403 (2013). http://dx.doi.org/10.1155/2013/923403.

[46] Liang J, Huang Y, Zhang L, Wang Y, Ma Y, Guo T, Chen Y. Molecular-level dispersion of graphene into poly (vinyl alcohol) and effective reinforcement of their nanocomposites. Adv Funct Mater, **19,** 2297 (2009). http://dx.doi.org/10.1002/adfm.200801776.

[47] Hu W, Peng C, Luo W, Lv M, Li X, Li D, Huang Q, Fan C. Graphene-based antibacterial paper. ACS Nano, **4,** 4317 (2010). http://dx.doi.org/10.1021/nn101097v.